Tumor Biol. (2012) 33:2411–2421
DOI 10.1007/s13277-012-0505-1

RESEARCH ARTICLE

ENTPD5-mediated modulation of ATP results in altered metabolism and decreased survival in gliomablastoma multiforme

Sohila Zadran · Arash Amighi · Erick Otiniano · Kaylee Wong · Homera Zadran

Received: 8 August 2012 / Accepted: 28 August 2012 / Published online: 20 September 2012

Abstract Gliomablastoma multiforme (GBM) is the most aggressive of brain cancers in humans. Response to current therapies remains extremely poor, with dismal survival statistics. Recently, the endoplasmic reticulum UDPase, ectonucleoside triphosphate diphosphohydrolase 5 (ENTPD5), was identified as a key component in the Akt/phosphatidylinositol 3-kinase/phosphatase and tensin homolog regulatory loop, capable of synergizing aerobic glycolysis and cancer cell proliferation in vitro. Utilizing a novel enhanced acceptor fluorescence-based single-cell adenosine 5′-triphosphate (ATP) biosensor, we analyzed ENTPD5-mediated modulation of cytosolic ATP. Here, ENTPD5-dependent modulation of cellular ATP in GBM results in altered metabolic kinetics in vitro, increasing the catabolic efficiencies of aerobic glycolysis and fatty acid oxidation. Additionally, an upregulation of ENTPD5 in both GBM mouse xenografts and in GBM patient tumors was identified, resulting in dramatically reduced survival. Therefore, these results not only provide new tools to monitor ATP flux and cellular metabolism kinetics but also identified a novel therapeutic target for GBM.

Keywords ENTPD5 · Single-cell EAF-based ATP sensor · Metabolomics · Glioblastoma multiforme

Statement of significance: Utilizing a novel enhanced acceptor fluorescence-based single-cell ATP biosensor, ENTPD5-mediated modulation of cytosolic ATP alters metabolic kinetics. ENTPD5 is identified as a new therapeutic target for GBM.

S. Zadran (✉) · A. Amighi · E. Otiniano · K. Wong · H. Zadran
David Geffen School of Medicine,
University of California, Los Angeles,
10833 Le Conte Ave., Center for the Health Sciences,
Room CHS 33-165,
Los Angeles, CA 90095, USA
e-mail: szadran@mednet.ucla.edu

Introduction

Glioblastoma multiforme (GBM) is an aggressive primary brain tumor that exhibits extremely poor response to current therapies. Despite maximal therapy with surgical resection, radiation, and temozolomide, survival statistics remain dismal. GBM are very vascular tumors with remarkable molecular and genetic heterogeneity. Phosphatidylinositol 3-kinase (PI3K) signaling is hyperactivated in nearly 90 % of GBMs, most frequently in association with epidermal growth factor receptor amplification and mutation and loss of the phosphatase and tensin homolog (PTEN) tumor suppressor protein. Additionally, GBM has a strong glycolytic phenotype, with GBM U87 and U87vIII cells lines displaying both a high glycolytic rate with increased lactic acid production and impaired mitochondrial respiratory function [1, 2].

Warburg first demonstrated that the metabolism of cancer cells, even under normoxia, is characterized by an increase in the ratio of cytoplasmic glycolysis to mitochondrial glucose oxidation [3]. Although the precise mechanism remains unknown, the metabolic switch from mitochondrial glucose oxidation to cytoplasmic glycolysis, even in the presence of oxygen, may offer cancer cells a proliferative advantage [4]. Recent studies have identified a correlation between signaling pathways regulating metabolism and cell proliferation [5]. Proliferating cells adapt to facilitate the uptake of nutrients for additional cell growth. Glycolysis-mediated lactic acid production promotes angiogenesis, interstitial matrix breakdown, and facilitates metastasis [6]. Most glycolytic enzymes also have direct antiapoptotic actions, and decreased mitochondrial function is associated with inhibition of mitochondrial-dependent apoptosis [7]. Additionally, studies in prostate cancer associated modulation in fatty acid metabolism to cancer progression. Several enzymes involved in the

fatty acid metabolism pathways are altered in prostate cancers when compared to normal prostate [8]. These metabolic deficiencies may allow for tumor cells to be isolated from normal cells, providing metabolism-specific targets for therapeutics.

In contrast to normal cells, which metabolize ketone bodies for energy during reduced glucose levels, GBM cells are incapable of metabolizing ketone bodies for energy and are dependent on glycolysis for both survival and proliferation [9]. Several of the molecular abnormalities that occur in GBM are also suppressants of mitochondrial glucose oxidation and promoters of cytoplasmic glycolysis. PI3K signaling has been implicated in the altered glucose metabolism of cancer cells including GBM, and the serine/threonine kinase Akt, a major PI3K effecter, promotes glucose uptake and increases the activity of glycolytic enzymes in several cancers [10]. Recently, it has been shown that Akt signaling leads to increased aerobic glycolysis via PI3K-mediated upregulation of the endoplasmic reticulum (ER) UDPase enzyme, ectonucleoside triphosphate diphosphohydrolase 5 (ENTPD5), implicating ENTPD5 as a key component in the PI3K/PTEN regulatory loop [11].

ENTPD5 utilizes the hydrolysis of UDP to UMP to promote *N*-glycosylation and folding of glycoproteins in the ER. ENTPD5 is also believed to mediate the enhanced ability for cancer cells to generate adenosine monophosphate (AMP) from adenosine 5′-triphosphate (ATP) and increased glucose entry into glycolysis in PTEN-deficient cells [12]. Therefore, ENTPD5 was considered a critical determinant of the catabolic efficiency of glycolysis. Utilizing a novel enhanced acceptor fluorescence (EAF)-based single-cell ATP biosensor, ENTPD5-mediated modulation of cytosolic ATP was analyzed. These results demonstrate for the first time an ENTPD5-dependent increase of ATP flux in GBM. This ENTPD5-mediated modulation of cytosolic and whole cell ATP levels resulted in altered metabolic kinetics in vitro, increasing both the catabolic efficiencies of both aerobic glycolysis and altering fatty acid oxidation capacity under glucose-deprived conditions. Additionally, an upregulation of ENTPD5 in both GBM mouse xenografts and in GBM patient tumors was identified, resulting in dramatically reduced survival in patients exhibiting elevated tumor ENTPD5 expression, providing an innovative therapeutic metabolic target in GBM.

Results

Characterization of EAF-based single-cell ATP sensor

Adenosine 5′-triphosphate is a critical regulator of cellular metabolism and signaling [13]. To monitor ATP flux on a single-cell level and in real-time in vitro, a genetically encoded enhanced acceptor fluorescence-based ATP biosensor was developed. This ATP biosensor utilizes a modified mimic of the ε subunits of the *Bacillus subtilis* F_0F_1 synthase. This ε subunit was chosen for its ability to bind ATP without hydrolyzing it [14]. Additionally, this EAF-based ATP sensor utilizes EAF pairs capable of enhanced acceptor fluorescence [15]. Unlike traditional fluorescence resonance energy transfer (FRET) pairs, in which donor emission must overlay acceptor excitation [16], we utilized the fluorophores, green fluorescent protein (GFP), and yellow fluorescent protein (YFP). Both GFP and YFP are excited at similar excitation wavelengths, and upon ATP binding, the sensor will undergo EAF, emitting an enhanced fluorescence signal. The EAF-based ATP sensor was genetically linked to GFP at the C-terminus and YFP at the N-terminus. Additionally, four hydrophobic amino acid residues forming a hydrophobic surface were replaced by hydrophilic residues to retard nonspecific hydrophobic interactions with other cellular proteins, such as the F_0F_1 synthase [14].

Single-cell ATP sensor specifically monitors levels of cytosolic ATP in vitro

ATP flux was visualized in single U87 and U87vIII GBM cell lines expressing the EAF-based ATP biosensor. Both EAF donor and EAF acceptor were monitored via confocal microscopy upon excitation with the 488-nm laser line. Both U87 and U87vIII GBM cell lines show strong EAF signal in the cytosol. Additionally, increased EAF was observed in U87vIII when compared to U87 cells (Fig. 1a), indicating increased levels of ATP in the cytosol in U87vIII cells. U87 and U87vIII cells expressing the EAF-based ATP sensor were also quantified for EAF signal via spectrofluorometric analysis. U87vIII cells exhibited almost a significant increase in EAF signal when compared to U87 cells (Fig. 1b).

ENTPD5 synergizes aerobic glycolysis and cell proliferation and modulates autophagy in U87 and U87vIII GBM cells

ENTPD5 was identified to promote *N*-glycosylation and aerobic glycolysis and is an integral component in the PI3K/PTEN regulatory pathway in vitro [17]. U87vIII, a PTEN null GBM cell line, exhibits elevated levels of phosphorylated Akt (pAkt) and p70S6 kinase [18]. Here, the presence of ENTPD5 in U87 cells and elevated levels of ENTPD5 in U87vIII cells is observed for the first time (Fig. 2a). To monitor the effect of ENTPD5 on ATP flux in U87 and U87vIII cells, modified monolayer-protected gold (MPG) nanoparticle delivery system was used to genetically knock down ENTPD5 in U87 and U87vIII cells expressing the EAF-based ATP sensor as described in the "Material and methods." Confocal images of single living

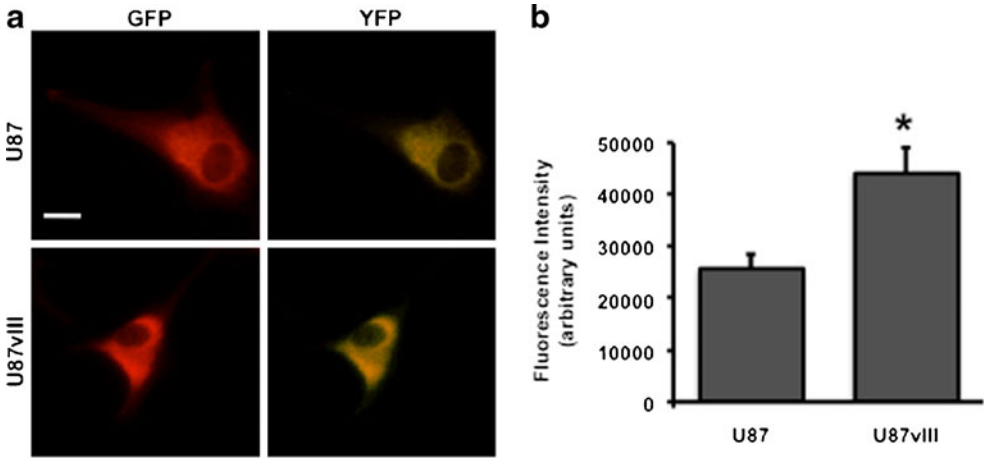

Fig. 1 EAF-based ATP sensor monitors cytosolic ATP on a single-cell level. **a** U87 and U87vIII GBM cells lines expressing the EAF-based ATP sensor was monitored via confocal microscopy upon excitation with the 488-nm laser line. *Scale bars*=20 μm. **b** Spectrofluorometric quantification of EAF in single living U87 and U87vIII cells. Data represent the mean of ± SEM of five independent experiments (statistical significance was assessed by Student's *t* test, where **p*< 0.05)

cells exhibited increase levels of cytosolic ATP levels in both U87 and U87vIII cells within 12 h of ENTPD5 knockdown. Pseudocolor saturation treatment of captured images was applied to highlight time- and treatment-dependent changes in EAF signal (Fig. 2b). To ensure that the modified MPG nanoparticle system utilized to effectively delivered

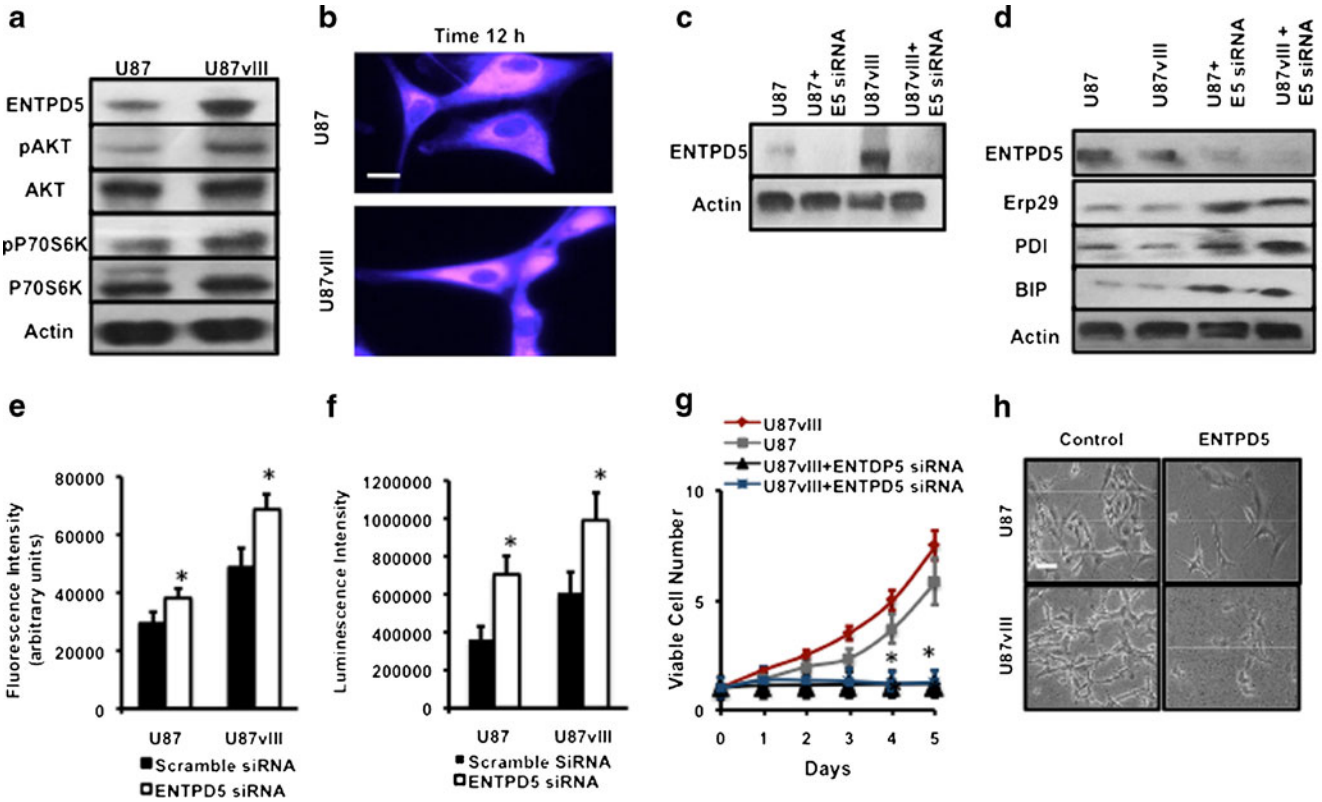

Fig. 2 ENTPD5 modulates ATP flux, autophagy, and proliferation in U87 and U87vIII. **a** Immunoblot analysis of ENTPD5, pAkt, Akt, pP70S6K, and P70S6K of whole cell extracts of U87 and U87vIII cells. **b** Modified MPG nanoparticle delivery system was used to genetically knock down ENTPD5 in U87 and U87vIII cells expressing the EAF-based ATP sensor. Confocal images of single living cells were captured 12 h following ENTPD5 knockdown. Representative images were captured on Leica image software and analyzed on ImageJ. Pseudocolor saturation treatment of captured images was applied to highlight time- and treatment-dependent changes in EAF signal (*scale bars*=20 μm). C. Immunoblot analysis of modified MPG nanoparticle system-mediated knockdown of ENTPD5 in whole cell extracts of U87 and U87vIII cells. **d** Immunoblot analysis of ENTPD5, EGFR, ERp29, PDI, and BiP in whole cell extracts of U87 and U87vIII pretreated with scramble or ENTPD5 siRNA. **e** U87 and U87vIII cells expressing the EAF-based ATP sensor pretreated with scramble siRNA or ENTPD5 siRNA were subjected to spectrofluorometric analysis. **f** Whole cell ATP levels of U87 and U87vIII cells pretreated with scramble or ENTPD5 siRNA were monitored using a modified luciferin/luciferase-based ATP assay. **g** Relative cell proliferation U87 and U87vIII cells pretreated with scramble siRNA and ENTPD5 siRNA. Data represent the mean of ± SEM of four independent experiments (statistical significance was assessed by Student's *t* test, where **p*<0.05). **h** Representative images of cell morphology and cell proliferation of U87 and U87vIII cells under light microscope (*scale bars*=20 μm)

ENTPD5 siRNA to U87 and U87vIII cells and genetically knocked down ENTPD5; pretreated U87 and U87vIII cells were subjected to western blot analysis for total levels of ENTPD5. Levels of ENTPD5 were significantly reduced in both U87 and U87vIII cells treated with the MPG-siRNA delivery complexes (Fig. 2c), and unlike traditional Lipofectamine-based siRNA delivery systems, no cell cytotoxicity was observed.

Glucose-regulated protein 78 (GRP78) or binding immunoglobulin protein (BiP) is an ER chaperone and regulator of unfolded protein response (UPR) [19]. Recently, an in frame splice variant of the epithelial growth factor receptor (EGFR), identified as mLEEK, was found overexpressed in several cancers. This variant is believed to function as a transcription factor to regulate genes involved in the cellular response to the ER stress and the UPR. This mLEEK provided a link between EGFR signaling and the UPR [20]. The levels of GRP78/BiP in U87 and U87vIII cells were therefore also examined. Although no significant difference in levels of GRP78/BiP was observed in U87 and U87vIII cells, levels of GRP78/BiP were greatly increased in the ENTPD5 knockdown. Inversely, total levels of EGFR were decreased in ENTPD5 knockdown. Levels of the endoplasmic reticulum protein 29 (ERp29) and protein disulphide isomerase (PDI) were also increased in U87 and U87vIII cells with ENTPD5 knockdown (Fig. 2d). ERp29 and PDI both have been implicated in the facilitating the processing and transport of proteins in the early secretory pathway [21]. Recent studies have also implicated increased expression of ERp29 and PDI in inhibiting both cell proliferation and suppression of tumorigenesis [22].

ENTPD5 has been critically implicated in the conversion of ATP to AMP, possibly through elevated ATPase activity [11]. Both U87 and U87vIII cells expressing the EAF-based ATP sensor displayed increase levels of EAF in ENTPD5 knockdown cells (Fig. 2e), indicating increase levels of cytosolic ATP. Since the EAF-based ATP sensor is limited to cytosolic ATP, whole cell ATP levels were monitored using a modified luciferin/luciferase-based ATP assay. Briefly, for this assay, cells were perforated with digitonin to reduce ATP loss in sample preparation for luciferin/luciferase-based ATP assay. U87 and U87vIII cells with the ENTPD5 displayed greater levels of whole cell ATP when compared to scramble controls (Fig. 2f).

Given the increase in cellular ATP and Erp29 levels in ENTPD5 knockout cells, cell proliferation was also examined. As expected, U87vIII cells proliferate faster than U87 cells, but proliferation was completely abrogated within 24 h of ENTPD5 knockout (Fig. 2g). U87 and U87vIII cell morphology was also observed under light microscope at 5 days following ENTPD5 knockdown and showed significant reduction in cell proliferation (Fig. 2h). Interestingly, cells also displayed changes in cell shape reminiscent of the dynamic changes exhibited by cells before undergoing autophagic cell destruction. To further examined this, electron micrographs of U87 and U87vIII cells were examined for autophagic vacuoles. Although no autophagic vacuoles were observed in U87 cells, U87vIII cells displayed several autophagic vacuoles. Knockdown of ENTPD5 in both U87 and U87vIII cells increased levels of autophagic vacuoles in the cell cytoplasm (Fig. 3), as compared to scramble-treated controls. U87 and U87vIII cells without ENTPD5 knockdown were also analyzed for total levels of LC3b and p62, markers of cellular autophagy. Both LC3b and p62 levels were increased in cells with ENTPD5 knockdown. Also, U87vIII cells displayed increase levels of p62 compared to U87 cells (Fig. 3b). Studies have previously implicated PI3 kinases and their downstream signal transduction components, Akt in suppressing autophagy, while PTEN acts as a negative regulator of the PI3 and an activator of autophagy [22]. ENTPD5 is a regulator of the PI3K/PTEN regulatory loop [17]. The presence of this autophagic vacuoles in U87 and U87vIII with ENTPD5 knockdown may indicate a new pathway for the induction of autophagy. In the ER, ER stress can activate the unfolded protein response to induce the expression of chaperones and proteins involved in the recovery process, thus initiating the assembly of preautophagosomal structures and autophagic vacuoles [23].

Levels of ENTPD5 were also examined in U87 and U87vIII mouse xenografts. As expected, both U87 and U87vIII xenografts displayed elevated ENTPD5 levels compared to normal tissue (data not shown). U87vIII also had significantly greater levels of ENTPD5 staining compared to U87 xenografts (Fig. 3c).

ENTPD5 modulates metabolism, fatty acid oxidation, and ATP flux in U87 and U87vIII cells

Most cancer cells perform aerobic glycolysis [3]. As previously discussed, U87vIII cells expressing the EAF-based ATP sensor show elevated levels of cytosolic ATP and ENTPD5. Cellular respiration was measured as described in the "Material and methods." Briefly, cellular respiration was measured using the XF24 Extracellular Flux Analyzer (Seahorse Bioscience), in which continuous measurements of oxygen consumption rate (OCR) and extracellular acidification rate (ECAR) were collected over time. Basal ECARs were lower in both U87 and U87vIII cells with ENTPD5 knockdown, indicating decreased aerobic glycolysis (Fig. 4a). Oligomycin is an inhibitor of ATP synthase F_0 subunit, preventing the oxidative phosphorylation of ADP to ATP, which allows for monitoring of cellular ATP flux. As expected, injection of oligomycin increased ATP flux in both U87 and U87vIII cells with ENTPD5 knockdown (Fig. 4b). These cells also displayed decreased glucose consumption (Fig. 4e) and decreased lactate production (Fig. 4f) compared to control U87 and U87vIII cells as analyzed as

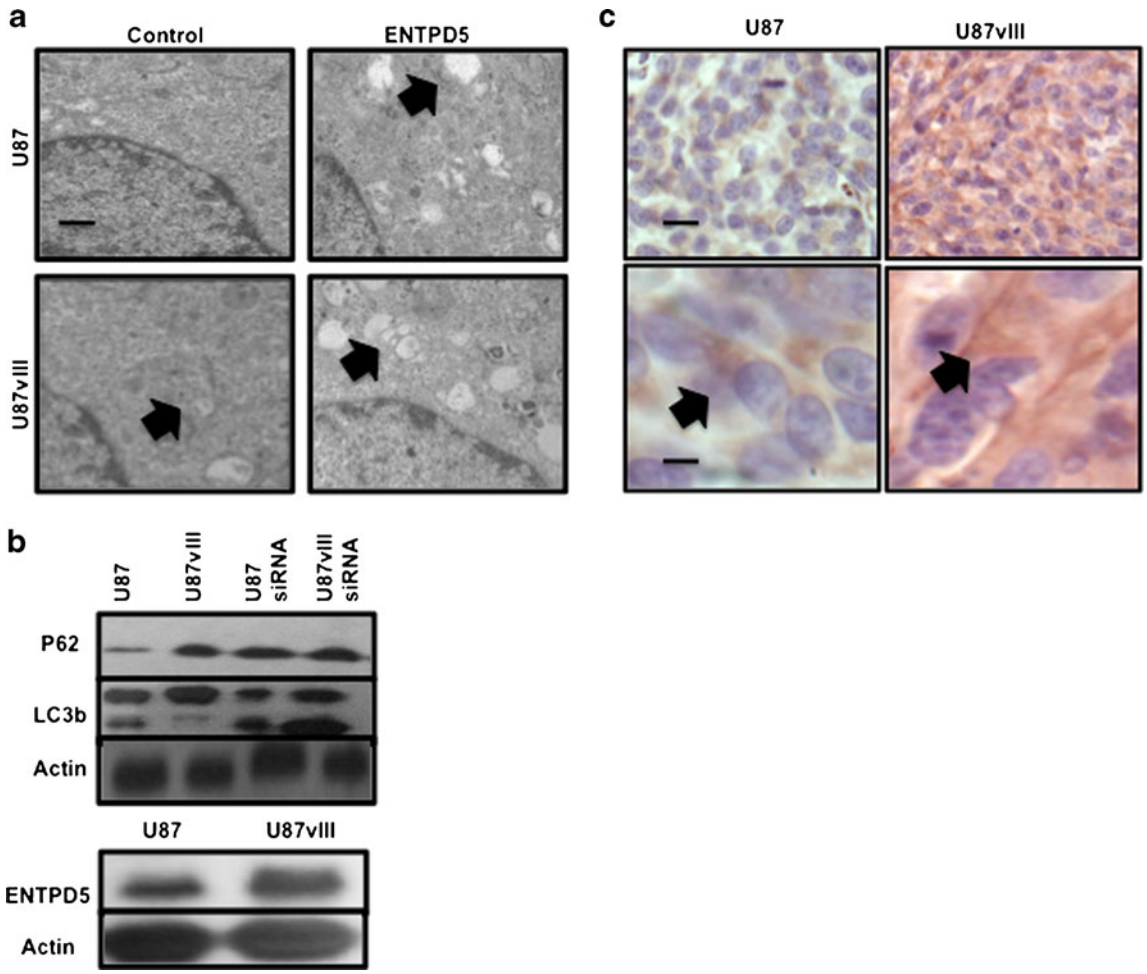

Fig. 3 ENTPD5 regulates autophagy in GBM cells. **a** Representative electron micrographs of U87 and U87vIII cells pretreated with scramble or ENTPD5 siRNA. *Arrows* indicate autophagic vacuoles. *Scale bar*=14 K/μM. **b** Representative image of U87 and U87vIII xenografts immunostained for ENTPD5. *Scale bars*=40 μm (*top*) and 20 μm (*bottom*). **c** Immunoblot analysis of ENTPD5 in U87 and U87vIII xenograft lysates (*bottom*) and of P62 and LC3b in whole cell extracts of U87 and U87vIII pretreated with scramble or ENTPD5 siRNA (*top*)

described in the "Material and methods," further implicating ENTPD5 in driving the catabolic efficiency of aerobic glycolysis.

In addition to altered glucose metabolism in human cancer, there is often a correlated increase in fatty acid turnover, oxidation, and clearance. The capacity of U87 and U87vIII cells to perform fatty acid oxidation was then monitored. Briefly, cells were transferred into low glucose media for 1 h prior to OCR readings. To further drive fatty acid oxidation, two injections of palmitate were administered. Fatty acid oxidation was monitored, and ANOVA was conducted to determine differences between groups. ENTPD5 knockdown reduced fatty acid oxidation capacity in both U87 and U87vIII cells (Fig. 4c). U87 and U87vIII cells expressing the EAF-based ATP sensor were also transferred to low glucose for 1 h and treated with palmitate. ATP levels were monitored within 30 min of treatments. Both U87 and U87vIII cells with ENTPD5 displayed decreased levels of cytosolic ATP (Fig. 4d).

Pyruvate (derived from glycolysis) and α-ketoglutarate (derived from glutaminolysis) are anaplerotic substrates for efficient Krebs cycle use of fatty acid-derived acetyl CoA; in certain cell types, high rates of aerobic glycolysis or glutaminolysis may promote efficient fatty acid oxidation [24]. Recently, it has been reported that 60 % of carbon skeletons from glucose are used for de novo fatty acid synthesis, which suggest that glycolysis may also be supporting fatty acid oxidation by contributing to fatty acid pool [25].

ENTPD5 expression is correlated with decrease survival in GBM

To further examine the role of ENTPD5 in human GBM, surrogate cancer-associated biomarkers, as well as levels of ENTPD5, were examined in tumor tissue samples, and adjacent normal brain from 140 patients arrayed on two-tissue microarrays. Staining and scoring of ENTPD5 was performed as described in the "Material and methods."

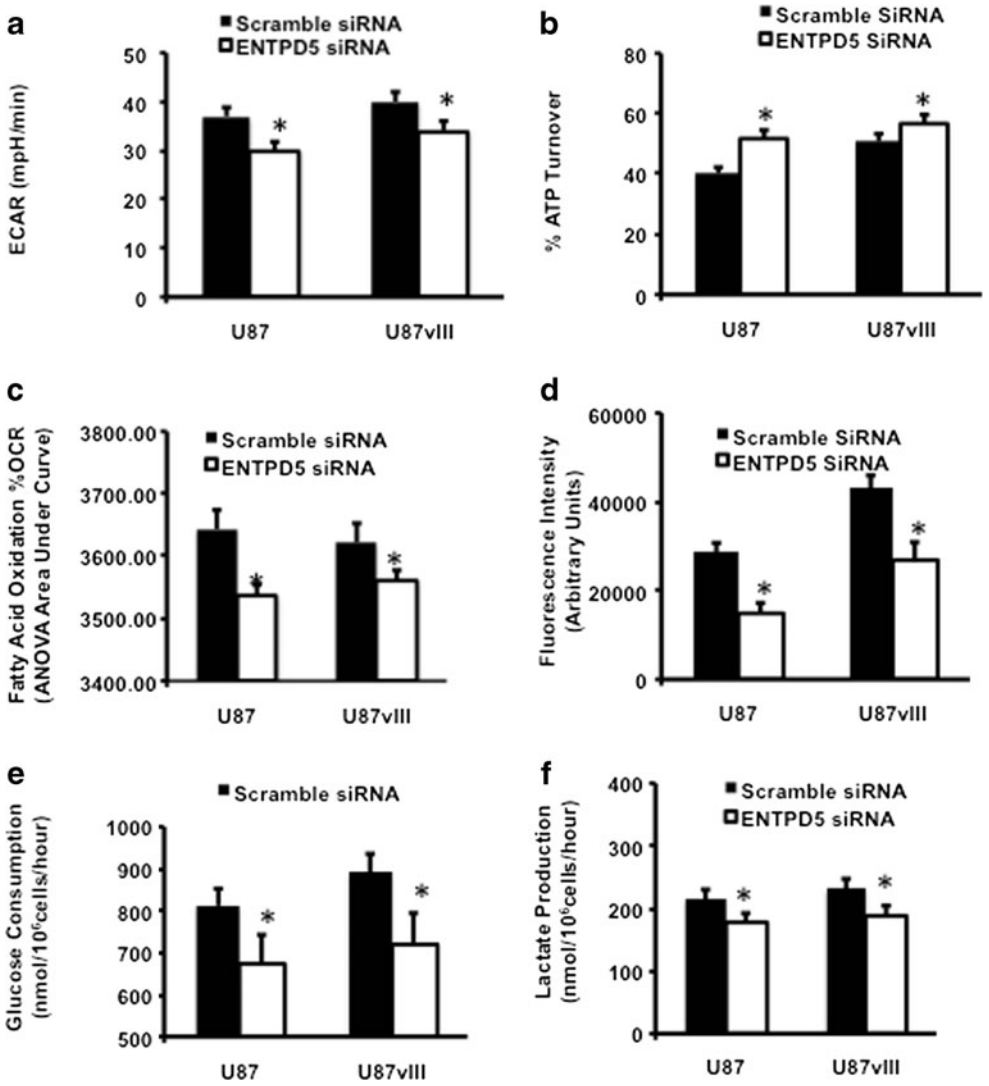

Fig. 4 ENTPD5-mediated modulation of GBM bioenergetics. **a** Basal ECAR levels of U87 and U87vIII cells pretreated with scramble siRNA or ENTPD5 siRNA. Data represent the mean of ± SEM of six independent experiments (statistical significance was assessed by Student's *t* test, where $*p<0.05$). **b** Percentage of ATP flux of U87 and U87vIII cells pretreated with scramble and ENTPD5 siRNA. Data represent the mean of ± SEM of six independent experiments (statistical significance was assessed by Student's *t* test, where $*p<0.05$). **c** Fatty acid oxidation of U87 and U87vIII cells pretreated with ENTPD5 or scramble siRNA. Data represent the mean of ± SEM of six independent experiments (statistical significance was assessed by ANOVA, where $*p<0.05$). **d** U87 and U87vIII cells expressing the EAF-based ATP sensor were conditioned in low-glucose media for 1 h prior to treatment with palmitate. EAF signal was monitored and quantified via spectrophotometry. Data represent the mean of ± SEM of four independent experiments (statistical significance was assessed by Student's *t* test, where $*p<0.05$). **e** Glucose consumption rate of U87 and U87vIII cells pretreated with scramble or ENTPD5 siRNA. Data represent the mean of ± SEM of four independent experiments (statistical significance was assessed by Student's *t* test, where $*p<0.05$). **f** Lactate production rate of U87 and U87vIII cells pretreated with scramble and ENTPD5 siRNA. Data represent the mean of ± SEM of four independent experiments (statistical significance was assessed by Student's *t* test, where $*p<0.05$)

Elevated ENTPD5 levels were observed in GBM cores compared to adjacent normal tissues (Fig. 5a), and over 68 % of GBMs displayed elevated ENTPD5 levels. The detection of these biomarkers significantly correlated with ENTPD5 detection (Fig. 5a). ENTPD5 showed strong correlation to EGFR ($p<0.0024$), VEGF ($p<0.0034$), and p53 ($p<0.0068$). Also, both LDLR and SREBP1 correlated significantly to ENTPD5, further supporting our finding of ENTPD5 modulation of fatty acid oxidation in U87 and U87vIII cells (Table 1). Interestingly, no correlation was made between ENTPD5 and Rictor, indicating that ENTPD5-mediated events may be mTOR independent. Density enhanced phosphatase-1, a tumor suppressor that negatively regulates cell proliferation [28], which also showed strong correlation with ENTPD5 ($p>0.0087$). Tumor and normal tissue samples were also randomly collected from several patients and subjected to western blotting analysis of ENTPD5 levels. All samples collected showed elevated levels

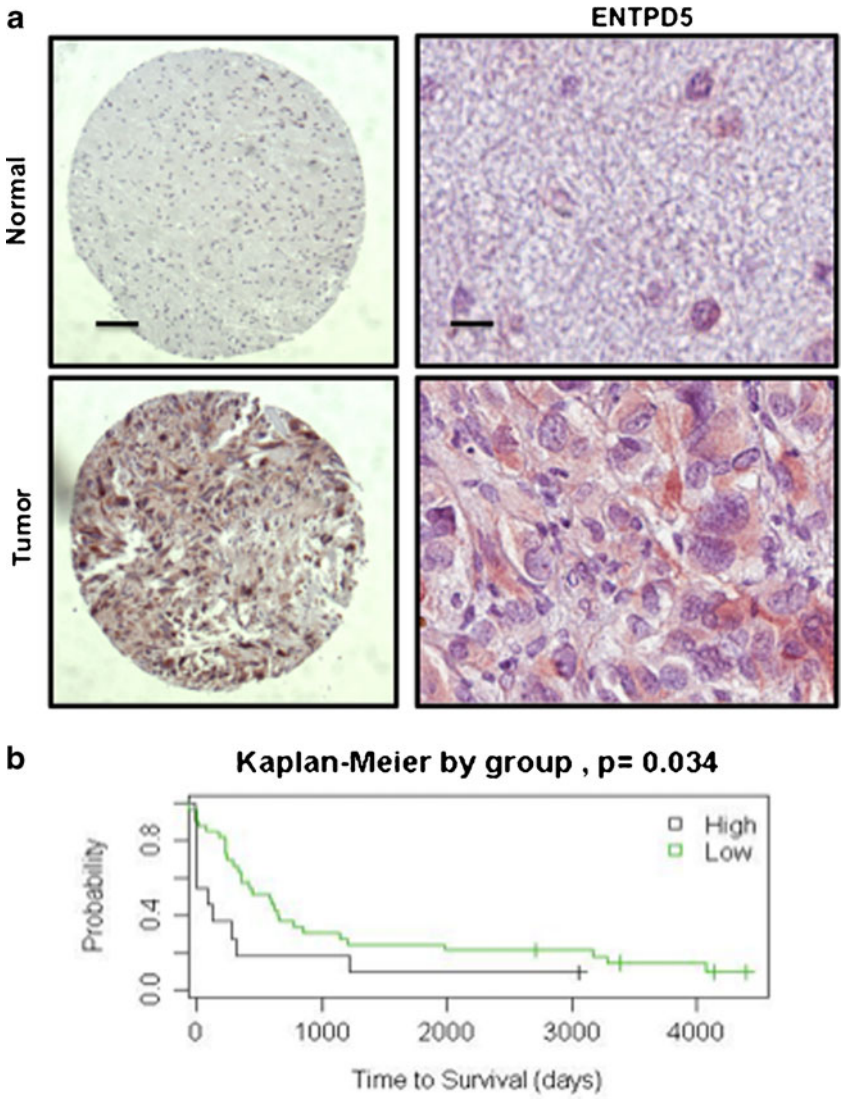

Fig. 5 Elevated levels of ENTPD5 reduce survival in GBM. **a** Immunohistological images of ENTPD5 staining in two TMAs comprising 252 tumor cores from 140 primary GBM patients. Tumor and normal tissue are counterstained with hematoxylin. *Scale bars*= 20 and 40 μm. **b** Representative Kaplan–Meier survival curves of 160 GBM patients as assessed. Statistical significance was assessed by Student's *t* test, **p*=0.034

of ENTPD5 in tumor samples, but not in normal tissue (data not shown). Real survival curves of over 165 GBM patients were also calculated using the Kaplan–Meier method. Patients with high expression of ENTPD5 showed significantly ($p<$ 0.034) reduced survival rates compared to patients with lower expression of ENTPD5 (Fig. 5b).

Discussion

ENTPD5 is a member of the ectonucleoside triphosphate diphosphohydrolase family, which consists of seven other members. The functions of these organelle-associated ENTPDases are still largely unexplored. Although in vitro data has implicated ENTPD5 in regulating both the PI3K/PTEN/Akt signaling loop and cellular bioenergetics, the role of ENTPD5 in GBM was largely unknown. The experimental data reported here identify ENTPD5 as a critical modulator of GBM bioenergetics and patient survival.

This innovative EAF-based ATP sensor monitored ENTPD5-mediated changes in cytosolic ATP in vitro in both GBM U87 and U87vIII cells. The sensor's functionality and sensitivity provide real-time analysis of cytosolic ATP flux on a single-cell level. Additionally, the sensor can be manipulated to monitor mitochondrial, nuclear, and ER ATP flux. Use of this sensor revealed that ENTPD5 increases both ATP flux and the catabolic efficiency of glycolysis in GBM U87 and U87vIII cells. Furthermore, these finding also indicates, for the first time, a role for ENTPD5 in fatty acid oxidation. Both U87 and U87vIII cells displayed reduced fatty acid oxidation capacity when ENTPD5 was knocked down. Expression of ENTPD5 was elevated in U87vIII cells and in patient tumor samples. Elevated ENTPD5 levels were observed in GBM core compared to adjacent normal tissues, and over 68 % of GBM cores displayed elevated ENTPD5 levels. GBM patients with high expression of ENTPD5 showed significantly reduced survival rates compared to patients with lower

Table 1 ENTPD5 correlates with cancer-associated markers

Symbol	Pearson's *r*	*p* value	Correlation
EGFR	0.2039	0.0004	Yes
ACC	0.1229	0.0342	Yes
DEP1	0.1520	0.0087	Yes
EMP2	0.2889	0.0001	Yes
FAS	0.1449	0.0124	Yes
KI67	0.2277	0.0001	Yes
LDLR	0.1615	0.0053	Yes
COOL2	0.0049	0.9327	No
P21	0.1542	0.0078	Yes
P53	0.1568	0.0068	Yes
pAkt	0.1629	0.0049	Yes
PEGFR	0.1777	0.0021	Yes
pMET	0.0813	0.1620	No
PML	0.2384	0.0001	Yes
PNDRG1	0.0359	0.5371	No
PP65	0.0786	0.1763	No
PPDGFR	0.0858	0.1401	No
PTB	0.1055	0.0694	No
PTEN	0.0314	0.5895	No
RICTOR	0.0264	0.6496	No
SREBP1	0.1875	0.0012	Yes
VEGF	0.1505	0.0094	Yes

Immunohistological analysis of TMAs was based on correlations of various cancer-associated markers. Pearson's *p* values were obtain to determine statistical significance and are indicated in the table

expression of ENTPD5. In summary, those results identify ENTPD5 as a novel therapeutic target in GBM.

Material and methods

All animal and human experimental procedures were conducted in accordance with the National Institutes of Health's *Guide for the Care and Use of Laboratory Animals* and with protocols approved by the Institutional Animal Care and Use Committee of the University of California, Los Angeles. Informed consent was obtained in written form from all human subjects and families of autopsy patients. Efforts were made to minimize animal suffering and numbers of mice used in the work described.

Cell lines

Mammalian cell lines described in this study were purchased from American Type Culture Collection (Manassas, VA). U87 and U87-EGFRvIII (also referred to U87vIII) GBM cell lines were obtained from the University of California, Los Angeles (UCLA) Brain Tumor Translational Resource. Cell lines were cultured and maintained in DMEM (Cellgro) supplemented with 5 % FBS (Omega Scientific) and 100 U/mL penicillin and streptomycin (Gibco) in a humidified 5 % CO_2 incubator at 37 °C. All cells were cultured as adherent monolayers.

Reagents and antibodies

The following reagents were used at the doses indicated and as described in the text and figure legends: oligomycin (Sigma), digitonin (Sigma), luciferin (Sigma), luciferase (Sigma), and palmitate (Sigma). The following antibodies were also utilized and were purchased from cell signaling unless otherwise indicated: actin (1:1,000), pAkt (1:500), Akt (1:1,000), pP70SK (1:500), P70S6K (1:1,000), EGFR (1:1,000) (Invitrogen), ENTPD5 (1:1,000) (Novus Biologicals), Erp29 (1:1,000) (Abcam), PDI (1:1,000) (Novus Biologicals), BiP (1:1,000), P62 (1:1,500), and LC3b (1:1,000). ENTPD5 siRNA and scramble siRNA was purchased from Novus Biologicals.

Glucose consumption and lactate production assay

Cells were seeded in culture plates and cultured for 6 h to 75 % confluence. The culture medium was then changed, and cells were incubated for an additional 24 h. Culture media were then collected, and glucose consumption and lactate production were examined on a BioProfile FLEX Analyzer (Nova Biomedical). Units were normalized to cell number, as described in cell proliferation assay methods.

Cell proliferation assay

Cells were regularly seeded into three 6-well plates and incubated at 37 °C for 24 h. Cells were then cultured in serum-free medium for another 24 h and treated in fresh serum-free medium with siRNA treatments for 24 h. Cells were then washed with warm media and supplemented with fresh serum-free medium. Cell proliferation was monitored at 1, 2, 3, 4, and 5 days. At the end of each time period, the cells were trypsinized to produce a single-cell suspension, and the viable cell number in each well was counted using trypan blue (Gibco) to detect viable cells and a hemocytometer (LW Scientific).

Western blotting

Cells were seeded in 10-mm tissue culture dishes and grown to 80 % confluence for 24 h. The cells were then serum starved for 24 h. The cells were placed in serum-free medium with siRNA treatments for 24 h. Subsequently, cells were lysed, and protein concentrations were

determined with bovine serum albumin (BSA) as standard (BioRad). Equal amounts of cell protein lysate were separated on 10 % SDS-polyacrylamide gel (Invitrogen) electrophoresis, and the protein was transferred onto nitrocellulose membranes (GE Healthcare). After blocking with 3 % BSA, membranes were incubated with the appropriate dilution of primary antibody. Membranes were then incubated with a horseradish peroxidase-conjugated secondary antibody. Proteins were detected using the enhanced chemiluminescence detection system (Thermo Scientific).

Oxygen consumption and extracellular acidification rate

The oxygen consumption and ECARs of U87 and U87vIII were determined using the Seahorse XF Extracellular Flux Analyzer (Seahorse Bioscience). The extracellular flux analyzer allows for analyzing oxygen consumption and ECARs of a defined number of cells in a defined small volume of culture media in real time and for monitoring their response to drug treatment. Twenty-four-well plates (Seahorse Bioscience) were precoated with laminin (Sigma) to prevent cell deattachment for this assay. Briefly, each well of the 24-well plate was coated with 50 μL laminin diluted in phosphate-buffered saline (PBS) (10 μg/mL) overnight. The next day, the wells were washed three times with PBS, and cells were plated at a density of 30,000 cells/well and allowed to attach overnight in normal media. The following day, the adherent cells were washed, and fresh serum-free media with scramble or ENTPD5 siRNA were added and allowed to incubate for an additional 24 h. The cartridge was loaded to dispense metabolic inhibitors sequentially as specific time points: oligomycin (inhibitor of ATP synthase, 1 μM) or palmitate (inductor of fatty acid oxidation, 20 μM). Basal OCR and ECAR were measured, as well as the changes in oxygen consumption caused by the addition of the metabolic inhibitors described above. Several parameters were deducted from the changes in oxygen consumption.

Tissue microarrays and immunohistochemical staining

Tissue microarrays and immunohistochemical staining were used to analyze ENTPD5 in patient tissue. Tumor specimens were obtained according to a protocol approved by the institutional review board of UCLA. Briefly, tissue microarray enable tumor tissue samples from different patients to be analyzed on the same histological slide. We constructed the array with a 0.6-mm needle to extract three representative tumor tissue cores from each formalin-fixed, paraffin-embedded tissue block of glioblastoma. Tissue microarray slides were counterstained with hematoxylin to visualize nuclei. Expression analysis was performed by two individual experimenters who were unaware of the findings of the molecular analyses. Scores of 0 and 1 were considered "low expression," and a score of 2 was considered "high expression." Scores were analyzed, and a Pearson's r was conducted to identify correlations. The following markers were also examined: EGFR, ACC, DEP1, EMP2, FAS, Ki67, LDLR, COOL2, P21, P53, pAkt, pEFGR, pMET, PML, pNDGR1, pP65, pPDGFR, PTB, PTEN, RICTOR, SREBP1, and VEGF.

Total ATP measurements

In utilizing recombinant firefly luciferase and its substrate D-luciferin, total cellular ATP levels were quantified. Briefly, cells were grown in 96-well plates, and following siRNA treatments, cells were washed and incubated with digitonin (30 μM) for 20 min to permeabilize cell membranes at 37 °C. Cells were then subjected to both luciferase and D-luciferin. This assay is based on a simple luciferase reaction which requires ATP as a cofactor to produce luminescent light. Luminescence was monitored on a luminometer (emission maximum 560 nm). Utilizing a standard of known ATP concentration, cellular ATP levels were correlated to luminescence levels.

EAF-based ATP sensor construction

B. subtilis ε subunit cDNA was synthesized by GeneScript. The synthesized cDNA also has valine-9, leucine-42, phenylalanine-67, and leucine-78 mutations to disrupt a hydrophobic patch for interaction with the γ subunit of ATP synthase. The cDNA was either genetically linked via PCR ligation (N-terminus) to yellow fluorescent protein and (C-terminus) to green fluorescent protein and inserted into pRSET-B vector (Invitrogen) for purification purposes or inserted into the pAcGFP1-C vector (Clontech) to allow for a mammalian expression vector containing humanized codons. Enhanced acceptor fluorescence, an alternative approach to traditional FRET, was detected via excitation of the construct at the donor emission at 480 nm and monitoring acceptor emission at 520 nm.

Confocal microscopy

Cells were plated on a laminin-coated glass bottom dish and transfected with plasmid coding the EAF-based ATP sensor using FuGENE6 transfection reagent (Roche Diagnostics). Between 1 and 2 days after transfection, cells were subjected to confocal imaging. Wide-field observations of the cells were performed on a Nikon TE2000-PFS inverted fluorescence microscope (Nikon Instruments). The exposure times were 500 ms for GFP and YFP images. Cells were maintained on a microscope at 37 °C with a continuous supply of a 95 % air and 5 % carbon dioxide mixture by

using a stage-top incubator. Image analysis was performed using ImageJ. The YFP emission saturation was calculated by dividing pixel-by-pixel, a YFP image with a GFP image.

Transmission electron microscopy

Cells were fixed in 2.5 % glutaraldehyde and 4 % paraformaldehyde and incubated for 2 h at 4 °C. Samples were washed three times with phosphate buffer (pH 7.4), and post-fixed for 2 h in 1 % osmium tetroxide at 4 °C. The fixed mixtures were dehydrated using a graded concentration series of acetone, and embedded in Epon 812. Sections were made at 50–60 nm and stained with uranyl acetate followed by lead citrate. The samples were observed and photographed at 80 kV under a JEM 1010 transmission electron microscope.

Immunohistochemistry

Surgical GBM tissues were fixed in 10 % formaldehyde and embedded in paraffin. Slides were deparaffinized in xylene and rehydrated with ethanol. For the antigen retrieval, slides were immersed in 0.01 M citrate buffer (Thermo Scientific Fisher, Rockford, IL), pH 6, and heated with a microwave for 10 min. Peroxidase activity was quenched with 0.3 % hydrogen peroxide in methanol. After blocking for 1 h with 10 % normal goat serum, slides were incubated with rabbit antihuman polycolonal ENTPD5 antibody for 2 h at room temperature. Antibody binding was detected using EnVision + (goat, anti-rabbit, Dako), followed by Vector DAB substrate kit (Vector Laboratories, Burlingame, CA), and counterstained with hematoxylin.

Xenotransplantation of U87 and U87vIII GBM cells

Mice of 6–8 weeks of age (Charles River Laboratories, Wilmington, MA) were anesthetized with intraperitoneal administration of ketamine. GBM U87 or U87vIII were dissociated, and 500,000 cells were stereotactically transplanted in the right peritoneal cavity. After 3 weeks, the mice were culled, and tumors were extracted. Tumors were then subjected to fixation with 4 % paraformaldehyde, followed by hematoxylin staining.

Nanoparticle delivery of ENTPD5 siRNA

An altered MPG peptide was synthesized by solid-phase peptide synthesis according to Fmoc/tBoc method and purified. The modified MPG sequence is as follows: b-RRRRRRRAFLGWLGAWGTMGWSPKKKRK-CY. The parent MPG parent peptide was shortened by six residues, and a heptarginine motif was added to improve interactions with both siRNA and lipid phase of the membrane. A beta-alanine was also added to the N-terminus to allow further functionalization of the peptide. For transfection of ENTPD5 siRNA, cells were cultured in normal media for 24 h at 70 % confluence, then washed, and placed in serum-free media for 12 h. ENTPD5 siRNA (100 nM) was complexed with the modified MPG and a molar ratio of 1/20 for 30 min at 37 °C and added to the cells for 24 h. ENTPD5 protein levels were determined at 12 and 24 h following transduction via western blotting. Cells were also examined for viability via trypan blue uptake as previously described prior to ENTPD5 analysis and EAF studies.

Statistical analysis

Results are shown as mean ± standard error of the mean (SEM). Pearson's r was used to assess correlations between various markers on TMA. ANOVA was utilized to identify statistically significant differences between groups in the fatty acid oxidation experiments. Student's t test was utilized for all other experimental correlations. $p<0.05$ and $p<0.01$ were considered statistically significant.

Acknowledgments The technical aid of Shaojun Zhu, Huijun Yang, Dr. Sirus Kohan, and Ms. Birgitta Sjostrand in experiments was appreciated. Additionally, suggestions provided by Dr. Laurent Vergnes in XF Seahorse Analyzer experiments and Dr. Sergey Marniov and UCLA Brain Tumor Translational Resource for biospecimen and biorepository support were also greatly appreciated. The guidance and experimental suggestions were provided by Dr. James Heath and Dr. Raphael Levine for this project. The UCLA Department of Pathology and Laboratory Medicine and the David Geffen School of Medicine provided early career award and financial support for the project.

Conflicts of interest None.

References

1. DeAngelis LM. Brain tumors. N Engl J Med. 2001;344(10):114–23.
2. Parsons DW, Jones S, Zhang X, Lin JC, Leary RJ, Angenendt P, et al. An integrated genomic analysis of human glioblastoma multiforme. Science. 2008;321(10):1807–12.
3. Vander Heiden MG, Cantley LC, Thompson CB. Understanding the Warburg effect: the metabolic requirements of cell proliferation. Science. 2009;324(4):1029–33.
4. Locasale JW, Cantley LC, Vander Heiden MG. Cancer's insatiable appetite. Nat Biotechnol. 2009;27(3):916–7.
5. Metallo CM, Vander Heiden MG. Metabolism strikes back: metabolic flux regulates cell signaling. Genes Dev. 2010;24(10):2717–22.
6. Sjøbakk TE, Johansen R, Bathen TF, Sonnewald U, Kvistad KA, Lundren S, Gribbestad IS. Metabolic profiling of human brain metastases using in vivo proton MR spectroscopy at 3 T. BMC Cancer. 2007;7(8):141–5.
7. Mayevsky A. Mitochondrial function and energy metabolism in cancer cells: past overview and future perspectives. Mitochondrion. 2009;9(3):165–79.
8. Hsing AW, Sakoda LC, Chua Jr S. Obesity, metabolic syndrome and prostate cancer. Am J Clin Nutr. 2007;86(3):s843–57.

9. Shelton LM, Huysentruyt LC, Mukherjee P, Seyfried TN. Calorie restriction as an anti-invasive therapy for malignant brain cancer in the VM mouse. ASN Neuro. 2010;2(3):e00038.
10. Lino MM, Merlo A. PI3Kinase signaling in glioblastoma. J Neurooncol. 2010;103(3):417–27.
11. Fang M, Shen Z, Huang S, Zhao L, Chen S, Mak TW, Wang X. The ER UDPase ENTPD5 promotes protein *N*-glycosylation, the Warburg effect, and proliferation in the PTEN pathway. Cell. 2010;143(5):711–24.
12. Read R, Hansen G, Kramer J, Finch R, Li L, Vogel P. Ectonucleoside triphosphate diphosphohydrolase type 5 (Entpd5)-deficient mice develop progressive hepatopathy, hepatocellular tumors, and spermatogenic arrest. Vet Pathol. 2009;46(3):491–504.
13. Pellegatti P, Raffaghello L, Bianchi G, Piccardi F, Pistoia V, Di Virgilio F. Increased level of extracellular ATP at tumor sites: in vivo imaging with plasma membrane luciferase. PLoS One. 2008;3(7):e2599.
14. Imamura H, Huynh Nhat KP, Togawa H, Saito K, Lino R, Kato-Yamada Y, Nagai T, Noji H. Visualization of ATP levels inside single living cells with fluorescence resonance energy transfer-based genetically encoded indicators. Proc Natl Acad Sci USA. 2009;106(37):15651–6.
15. Calleja V, Ameer-Beg SM, Vojnovic B, Woscholski R, Downward J, Larijani B. Monitoring conformational changes of proteins in cells by fluorescence lifetime imaging microscopy. Biochem J. 2003;372(Pt 1):33–40.
16. Yuan J, Peng L, Bouma BE, Tearney GJ. Quantitative FRET measurement by high-speed fluorescence excitation and emission spectrometer. Opt Express. 2010;8(18):18839–51.
17. Shen Z, Huang S, Fang M, Wang X. ENTPD5, an endoplasmic reticulum UDPase, alleviates ER stress induced by protein overloading in Akt-activated cancer cells. Cold Spring Harb Symp Quant Biol. 2011;76(6):217–23.
18. Baldwin RM, Garratt-Lalonde M, Parolin DA, Krzyzanowski PM, Andrade MA, Lorimer IA. Protection of glioblastoma cells from cisplatin cytotoxicity via protein kinase Ciota-mediated attenuation of p38 MAP kinase signaling. Oncogene. 2006;25 (20): 2909–19.
19. Reddy RK, Mao C, Baumeister P, Austin RC, Kaufman RJ, Lee AS. Endoplasmic reticulum chaperone protein GRP78 protects cells from apoptosis induced by topoisomerase inhibitors: role of ATP binding site in suppression of caspase-7 activation. J Biol Chem. 2003;278(23):20915–24.
20. Piccione EC, Lieu TJ, Gentile CF, Williams TR, Connolly AJ, Godwin AK, Koong AC, Wong AJ. A novel epidermal growth factor receptor variant lacking multiple domains directly activates transcription and is overexpressed in tumors. Oncogene. 2012;31 (24):2953–67.
21. Shnyder SD, Mangum JE, Hubbard MJ. Triplex profiling of functionally distinct chaperones (ERp29/PDI/BiP) reveals marked heterogeneity of the endoplasmic reticulum proteome in cancer. J Proteome Res. 2008;7(8):3364–72.
22. Qi L, Wu P, Zhang X, Qiu Y, Jiang W, Huang D, Liu Y, Tan P, Tian Y. Inhibiting ERp29 expression enhances radiosensitivity in human nasopharyngeal carcinoma cell lines. Med Oncol. 2012;29 (2):721–8.
23. Ueno T, Sato W, Horie Y, Komatsu M, Tanida I, Yoshida M, Ohshima S, Mak TW, Watanabe S, Kominami E. Loss of Pten, a tumor suppressor, causes the strong inhibition of autophagy without affecting LC3 lipidation. Autophagy. 2008;4(5):692–700.
24. Yorimitsu T, Nair U, Yang Z, Klionsky DJ. Endoplasmic reticulum stress triggers autophagy. J Biol Chem. 2006;281:30299–304.
25. Liu Y. Fatty acid oxidation is a dominant bioenergetic pathway in prostate cancer. Prostate Cancer Prostatic Dis. 2006;9: 230–4.